DFT and DRIFTS Studies on the Adsorption of Acetate on the Ag/Al_2O_3 Catalyst

Hongwei Gao,*,† Tingxia Yan,‡ Yunbo Yu,§ and Hong He§

Institute of Watershed Science and Environmental Ecology, Wenzhou, Medical College, Zhejiang, 325035, China, State Property Administration Department, Wenzhou Medical College, Zhejiang, 325035, China, and Research Center for Eco-Environmental Sciences, Chinese Academy of Sciences, Beijing, 100085, China

Received: January 9, 2008; In Final Form: February 3, 2008

The adsorption of acetate species (CH_3COO^-) on the Ag/ Al_2O_3 catalyst has been studied using in situ diffuse reflectance infrared Fourier transform spectroscopy and Density functional theory (DFT). The geometrical structures and vibrational spectra were obtained at the PBE1PBE level of DFT and compared with the corresponding experimental values. Theoretical calculations show that the calculated IR spectra are in good agreement with the experimental spectroscopic results.

1. Introduction

The selective catalytic reduction of NO by hydrocarbons (HC-SCR of NO) is a potential method to control the emissions of pollutants from the diesel and lean-burn engine. The mechanism of HC−SCR of NO in the presence of excess oxygen over the Ag/Al_2O_3 has been proposed as follows:[1−5]

$$NO + O_2 + C_2H_5OH \rightarrow NO_x \text{ (nitrate in particular)} + C_xH_yO_z \text{ (acetate in particular)}$$

$$\rightarrow R{-}NO_2 + R{-}ONO \rightarrow {-}NCO + {-}CN + NO + O_2 \rightarrow N_2 \quad (1)$$

The adsorbed species on catalysts during the SCR of NO_x have been observed by many researchers using IR spectroscopy, and several intermediates have been proposed to take part in the reduction of NO_x, such as NO_3-,[6−8] CH_3COO-,[8−10] $R{-}NO_2$,[9−11] $R{-}ONO$,[9−11] and NCO.[6,7,10,12,13] IR spectra have shown that adsorbed nitrates (NO_3-) and acetate (CH_3COO-) were the predominant surface species during the SCR of NO_x on Al_2O_3 or Ag/Al_2O_3.[7,8,14,15]

However, the exact adsorption state and assignment of acetate species on the Ag/ Al_2O_3 catalyst surface are still not clear. Auxiliary computer simulation of IR spectra with DFT quantum mechanical methods affords highly powerful and reliable tools for analytical chemistry by means of in situ diffuse reflectance infrared Fourier transform spectroscopy (DRIFTS).

In this work, we report on studies of the adsorption of acetate species on the Ag/Al_2O_3 catalyst studied by an in situ DRIFTS method and DFT method in order to investigate the interaction of acetate species with the surface of catalyst. This study aims to utilize experiment and theory toward the understanding of the formation of acetate species on the Ag/Al_2O_3 catalyst and their involvement in the mechanism of the SCR of NO. A fundamental understanding of the mechanism of the SCR of NO is believed to be essential for the development of a catalyst and the improvement of the potential application.

* To whom correspondence should be addressed: Tel.: +86-577-86699570. Fax : +86-577-86699570. E-mail: gaohongw369@hotmail.com.
† Institute of Watershed Science and Environmental Ecology, Wenzhou, Medical College.
‡ State Property Administration Department, Wenzhou Medical College.
§ Chinese Academy of Sciences.

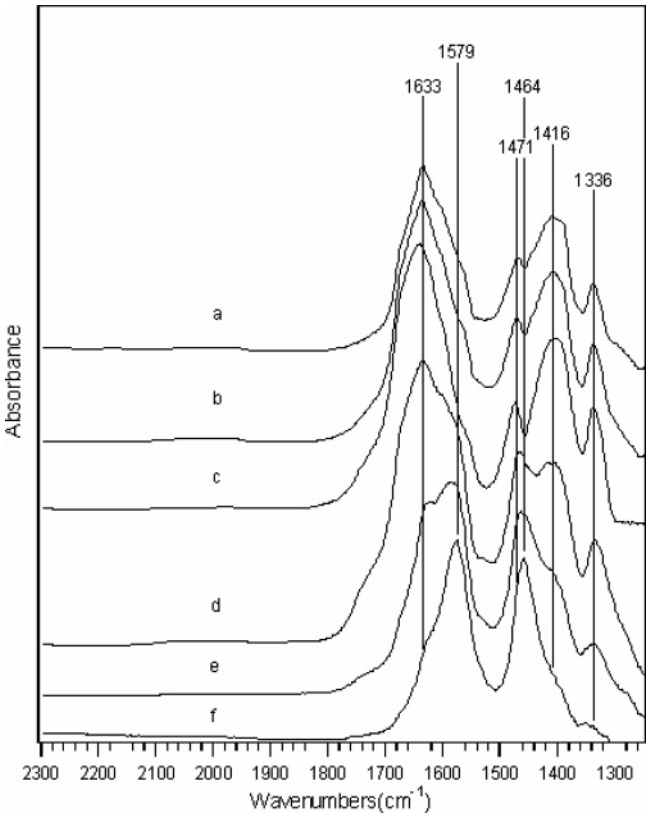

Figure 1. Experimental in situ DRIFTS spectra of adsorbed species in steady states on the Ag/Al_2O_3 catalyst in a flow of $C_2H_5OH + O_2$ at (a) 473K, (b) 523 K, (c) 573 K, (d) 673 K, (e) 773 K, and (f) 873 K. Conditions: C_2H_5OH 1565 ppm, O_2 10%.

2. Experimental Section

The Ag/Al_2O_3 catalyst (Ag loading is 5.0 wt %) was prepared by an impregnation of γ-Al_2O_3 powder (200 m^2/g) with an appropriate amount of silver nitrate aqueous solution. The sample was dried at 393 K for 3 h and calcined at 873 K for 3 h in the air.

DRIFTS spectra were recorded with a Nexus 670 (Thermo Nicolet) FT−IR, equipped with an in situ diffuse reflection chamber and a high sensitivity MCT detector. The Ag/Al_2O_3

10.1021/jp800177j CCC: $40.75
Published on Web 03/20/2008

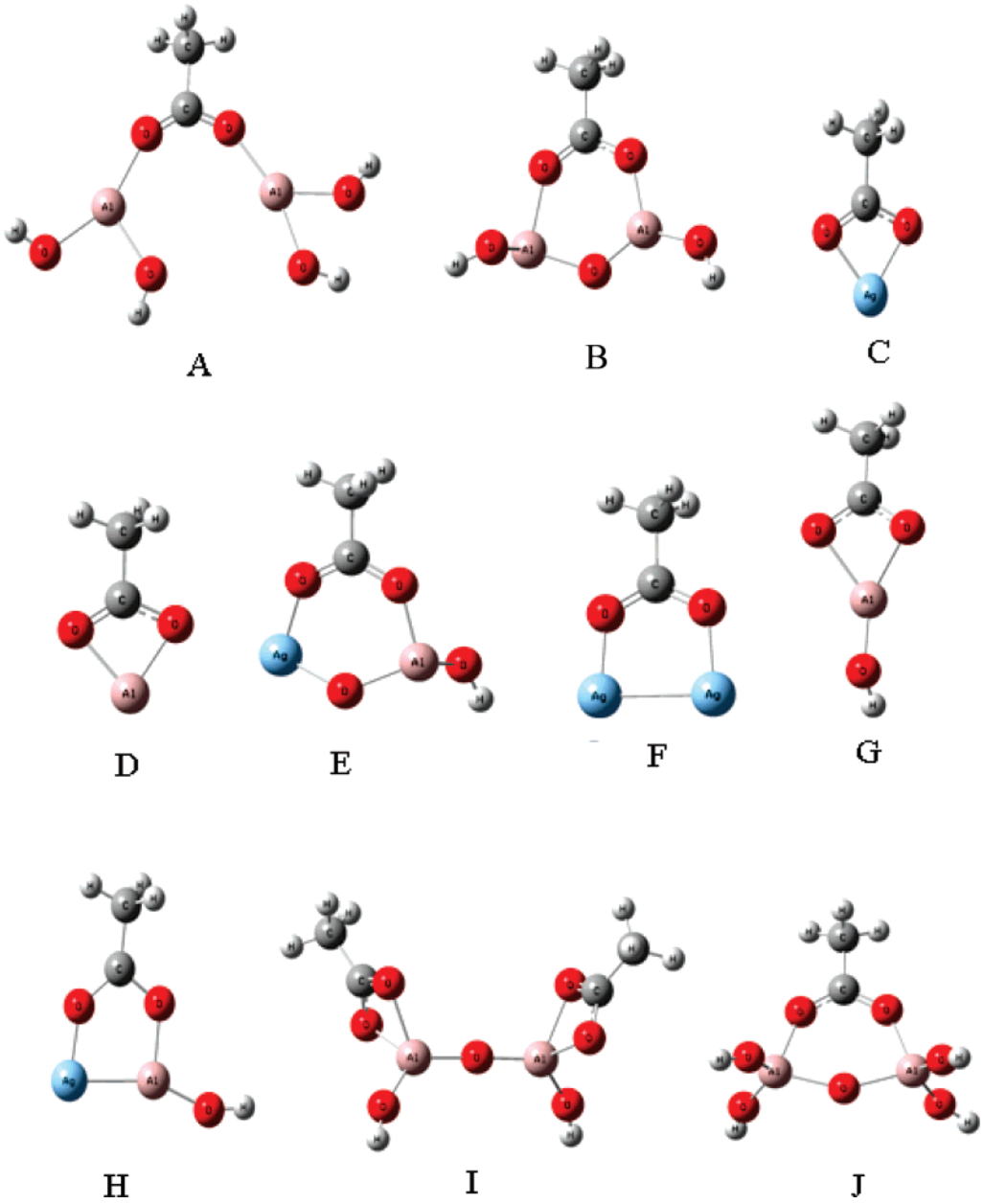

Figure 2. Optimized structure of the computational models (A−J) for enolic species on Ag/Al_2O_3 catalyst. Red circles represent O atoms; Black circles represent C atoms; White circles represent H atoms; Gray circles represent Al atoms.

catalyst for the in situ DRIFTS studies was finely ground and placed into a ceramic crucible in the in situ chamber. Mass flow controllers and a sample temperature controller were used to simulate the real reaction conditions, such as mixture of gases, pressure, and sample temperature. Prior to recording each DRIFTS spectrum, the sample was heated in situ in 10% O_2/N_2 flow at 873 K for 1 h and then cooled to the desired temperature for taking a reference spectrum. All gas mixtures were fed at a flow rate of 100 mL/min. All spectra were measured with a resolution of 4 cm^{-1} and with an accumulation of 100 scans.

3. Theoretical Section

All calculations were performed using the Gaussian98 program. The properties of the calculated models were determined through the application of density functional theory (DFT) using the PBE1PBE methods. The LANL2DZ effective core potential basis set was used for all of the calculations. The LANL2DZ basis replaces the 1s through 2p electrons of the heavy atoms with a potential field for a considerable computational savings. A double-ζ quality dunning basis was used for the light atoms and the remaining heavy atom electrons. Stability calculations confirmed the ground-state configuration of all of the wave functions. The calculated vibration frequencies and infrared intensity of the vibration normal modes using the Gaussian98 program are picked up by the GaussView 3.09 software package.

4. Results and Discussion

4.1. Experimental Spectra. Figure 1 shows the in situ DRIFTS of Ag/Al_2O_3 in a flow of C_2H_5OH (1565 ppm) + O_2

TABLE 1: Calculated Vibration Frequencies (in cm^{-1}) and IR Intensity (in km/mol) for the Calculated Models (A−J) at the PBE1PBE/LANL2DZ Level, and Corresponding Frequencies in the Experimental Gas-Phase Spectra

model	frequency (cm^{-1})	intensity (km/mol)	experiment (cm^{-1})	vibration mode
A	1599	389	1579	acetate species a-str.
	1454	345	1471−1464	acetate species str.
B	1616	372	1579	acetate species a-str.
	1452	218	1471−1464	acetate species str.
C	1524	80	1579	acetate species a-str.
	1467	381	1471−1464	acetate species str.
D	1525	57	1579	acetate species a-str.
	1488	254	1471−1464	acetate species str.
E	1619	351	1579	acetate species a-str.
	1446	218	1471−1464	acetate species str.
F	1528	31	1579	acetate species a-str.
	1479	128	1471−1464	acetate species str.
G	1522	77	1579	acetate species a-str.
	1422	241	1471−1464	acetate species str.
H	1669	189	1579	acetate species a-str.
	1332	432	1471−1464	acetate species str.
I	1537	126	1579	acetate species a-str.
	1449	486	1471−1464	acetate species str.
J	1582	500	1579	acetate species a-str.
	1482	166	1471−1464	acetate species str.

(10%) at a temperature range of 473−873 K in steady states. Exposure of this catalyst to the fed gas at 473 K resulted in the appearance of five peaks (1633, 1579, 1471−1464, 1416, and 1336 cm^{-1}). Peaks at 1579 and 1471−1464 cm^{-1} were assigned to ν_{as} (OCO) and ν_s (OCO) of acetate, respectively.[16−22] According to our earlier studies,[1] peaks at 1633, 1416, and 1336 cm^{-1} were assigned to asymmetric stretching vibration, symmetric stretching vibration, and C−H deformation vibration modes of an adsorbed enolic species, respectively. Apparently, the enolic species is predominant during the oxidation of C_2H_5-OH on the Ag/Al_2O_3 surface within a low-temperature range of 473−673 K. However, the surface acetate species becomes dominant at a high-temperature range of 773−873 K.

4.2. Geometry Optimization. The optimized structures of the calculation models (A−J) for the acetate species adsorption on the Ag/Al_2O_3 catalyst are shown in Figure 2. The equilibrium internuclear distance of the C−C single bond was equal to 1.4955−1.5082 Å, which is close to the experimental value of 1.50 Å. It was also found that the equilibrium internuclear distance of the C═O double bond was equal to 1.3054−1.3226 Å, which is in good agreement with the previously reported results.[16] The C−H bond length in acetate species for models (A−J) determined from DFT calculations is about 1.0884−1.0973 Å. The optimized distance between the oxygen atom and the aluminum atom in the models (A−J) is about 1.7139−1.7327 Å. The optimized bond length for the Ag−Al bond in model H is 2.4656 Å, whereas the optimized bond length for the Ag−Ag bond in model F is 2.7045 Å.

In calculated models (B−J), the optimized dihedral angles for the framework ring are little different. In these models, the optimized dihedral angles of D(COAlO) in model B, D(COAgO) in model C, D(COAlO) in model D, D(OAgOAl) in model E, D(OAgAgO) in model F, D(OAlOC) in model G, D(OAgAlO) in model H, D(COAlO) in model I and D(OAlOAl) in model J for the framework ring are 1.8627°, −0.01053°, 0.5607, 0.0000, −0.1148, 1.7349, 0.3086, 0.2020 and 3.5057°, respectively. These dihedral angles show that framework rings in these models are near to planar.

4.3. Comparison of Simulant Spectra with Experimental Ones. Calculated vibration frequencies (in cm^{-1}) and IR intensity (in km/mol) for the calculated models (A−I) at PBE1PBE/LANL2DZ level, and corresponding frequencies in the experimental gas-phase spectra are listed in Table 1. Simulant spectra for the models (A−J) are shown in Figures 3 and 4.

The calculated antisymmetric stretching vibrational modes of the adsorbed acetate species for the models (A−J) are 1599, 1616, 1524, 1525, 1619, 1528, 1522, 1669, 1537, and 1582 cm^{-1}, respectively (Figures 3 and 4). In comparison with the same experimental frequency of 1579 cm^{-1}, the error is on average about 20 cm^{-1} for model (A), 37 cm^{-1} for model (B), −55 cm^{-1} for model (C), −54 cm^{-1} for model (D), 40 cm^{-1} for model (E), −51 cm^{-1} for model (F), −57 cm^{-1} for model (G), 90 cm^{-1} for model (H), −42 cm^{-1} for model (I), and 3 cm^{-1} for model (J). Overestimation of experimental frequency values is about 1.27% for model (A), 2.34% for model (B), 2.53% for model (E), 5.70% for model (H) and 0.19% for model (J). Underestimation of experimental frequency values is about 3.42% for model (C), 3.42% for model (G), 2.66% for model (I). The calculated frequencies of model (J) at 1582 cm^{-1} with 500 km/mol intensity is relatively good matches of the most intense bands at 1579 cm^{-1} in the experimental spectrum (Figure 1).

The calculated symmetric stretching vibrational modes of the adsorbed acetate species for the models (A-J) are 1454, 1452, 1467, 1488, 1446, 1479, 1442, 1332, 1449, and 1482 cm^{-1}, respectively (Figures 3 and 4). For the same experimental frequency of 1471 cm^{-1}, the error is on average about −17 cm^{-1} for model (A), −19 cm^{-1} for model (B), −4 cm^{-1} for model (C), 17 cm^{-1} for model (D), −25 cm^{-1} for model (E), 8 cm^{-1} for model (F), −29 cm^{-1} for model (G), −139 cm^{-1} for model (H), −22 cm^{-1} for model (I), and 11 cm^{-1} for model (J). Underestimation of experimental frequency values is about 1.16% for model (A), 1.29% for model (B), 0.27% for model (C), 1.70% for model (E), 1.97% for model (G), 9.45% for model (H), and 1.50% for model (I). Overestimation of experimental frequency values is about 1.16% for model (D), 0.54% for model (F), and 0.74% for model (J). The symmetric stretching vibrational mode of the adsorbed acetate species of

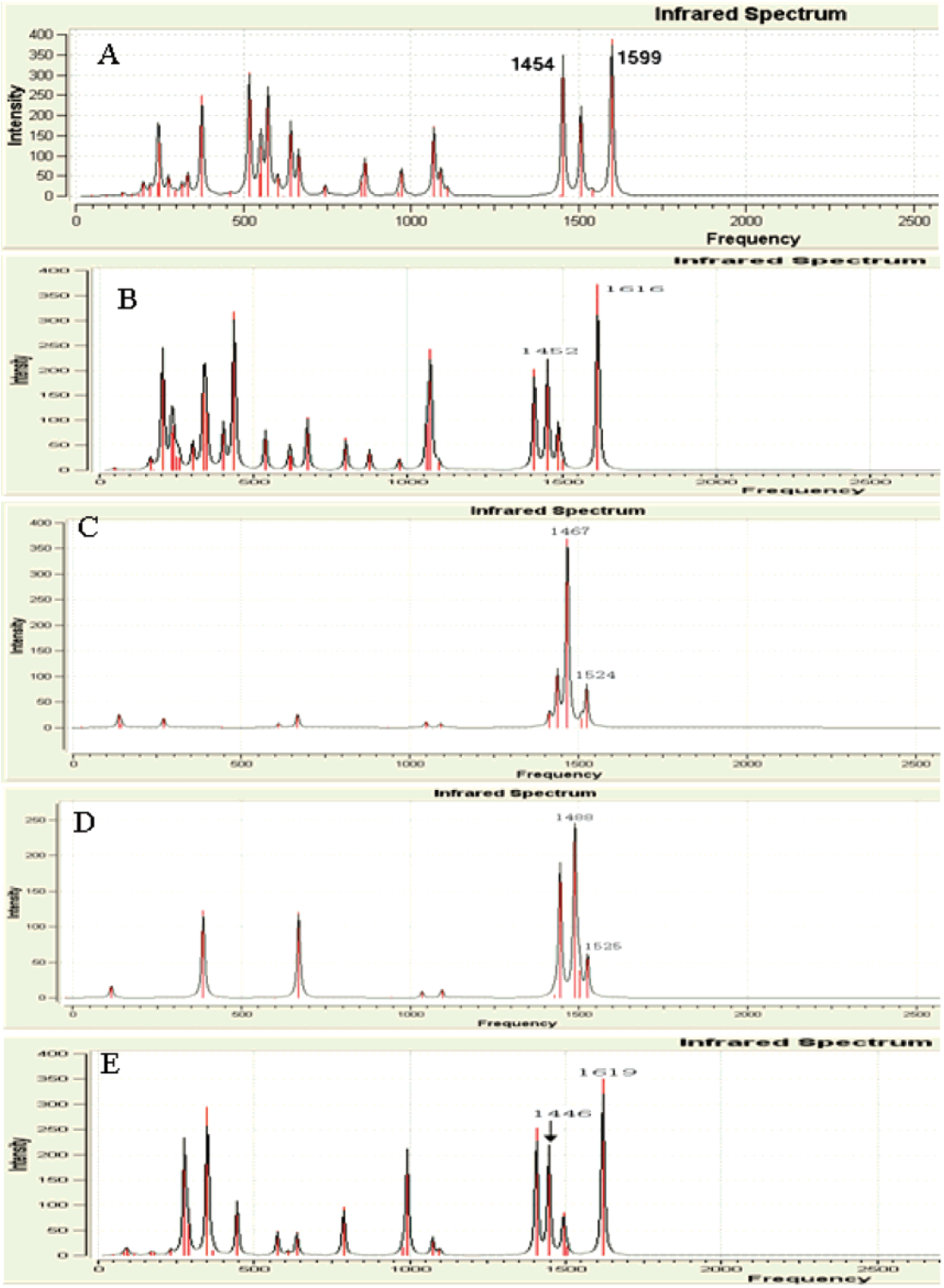

Figure 3. Calculated vibration IR spectra for the computational models (A−E) at PBE1PBE/LANL2DZ level.

model (J) calculated at 1482 cm^{-1} with 166 km/mol intensity is only 11 cm^{-1} higher than the experimental spectrum at 1471 cm^{-1} with strong absorbance within 0.74% error. The model (C) has the better result. The symmetric stretching vibrational mode of the adsorbed acetate species of model (C) calculated at 1467 cm^{-1} with 381 km/mol intensity is only 4 cm^{-1} lower than the experimental spectrum at 1471 cm^{-1} with strong absorbance within 0.27% error. The expressed frequencies at 1482 cm^{-1} for the model (J) and 1467 cm^{-1} for the model (C) in Figures 3 and 4 are relatively good matches of the most intense bands at 1471 cm^{-1} in the experimental spectrum (Figure 1).

Comparing model C with model J, although the calculated symmetric stretching vibrational mode of the adsorbed acetate species of model C is better than that of model J, there is big error between the calculated and experimental antisymmetric stretching vibrational modes of the adsorbed acetate species for model C. Therefore, the spectra of model J simulated by DFT-

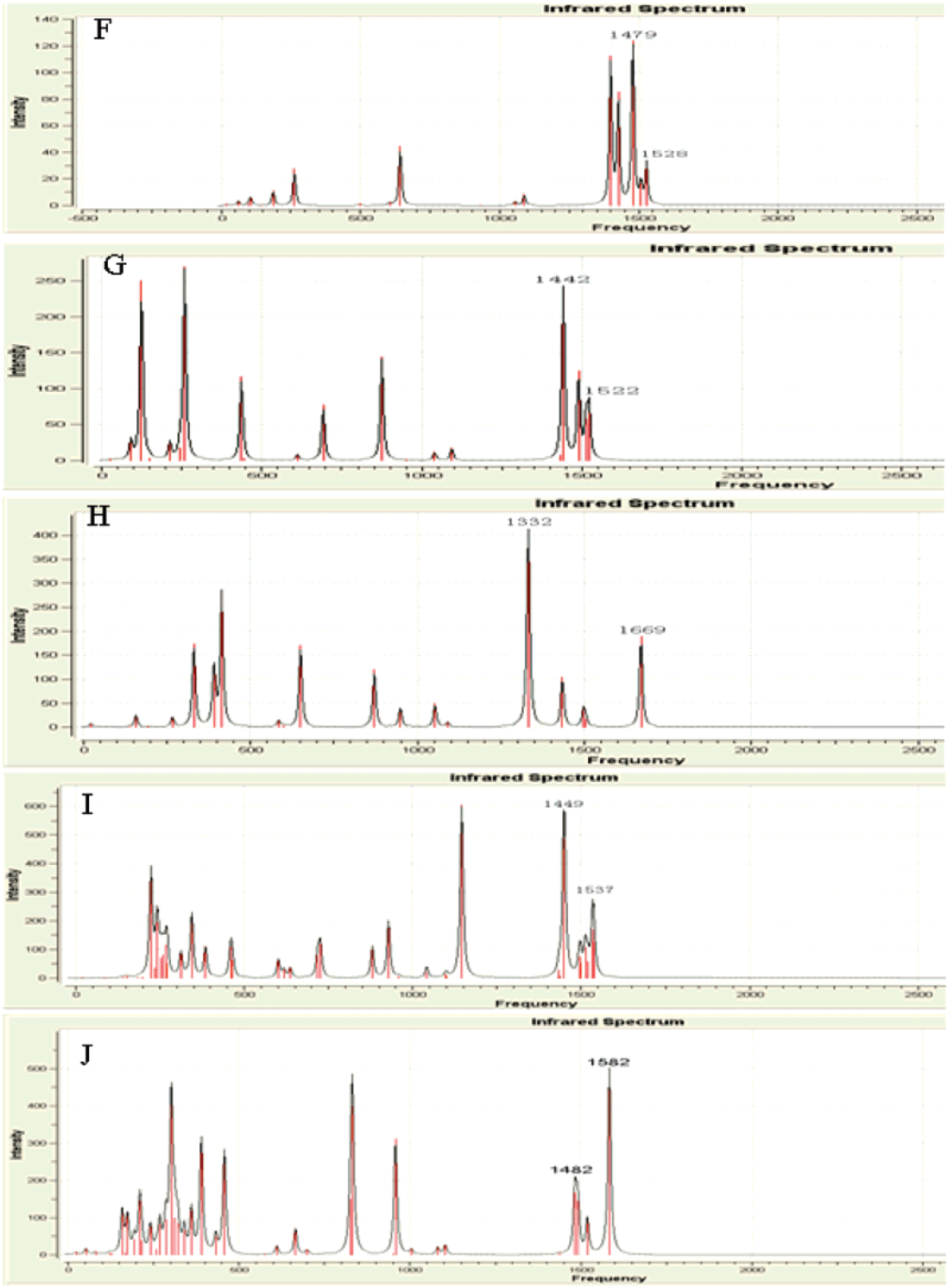

Figure 4. Calculated vibration IR spectra for the computational models (F−J) at PBE1PBE/LANL2DZ level.

PBE1PBE evidently best match the experimental counterparts for the overwhelming majority of the calculated models (A−J) considered in the present study.

5. Conclusions

The calculated IR spectrum for the model (J) is of reasonable similarity to the corresponding experimental spectrum. Furthermore, calculated antisymmetric and symmetric stretching vibrational modes of the adsorbed acetate species are in good agreement with the experimental data. The calculations clearly show that simulating infrared spectra with density functional theory (DFT) quantum mechanical method can be considered as the advantageous auxiliary tool for analyzing the mechanism of the acetate species adsorption over the Ag/Al_2O_3 catalyst.

Acknowledgment. This work was financially supported by the College Fund for Start-up Program of Wenzhou Medical College.

Note Added after ASAP Publication. Authors Y. Yu and H. He and their affiliation were added to the version published ASAP March 20, 2008; the corrected version was published ASAP April 4, 2008.

References and Notes

(1) Misono M.; Hirao Y.; Yokoyama C. *Catal. Today* **1997**, *38*, 157.
(2) Miller, J. T.; Glusker, E.; Peddi, R.; Zheng, T.; Regalbuto, J. R. *Catal. Lett.* **1998**, *55*, 15.
(3) Yan, Y.; Kung, H. H.; Sachtler, W. M. H.; Kung, M. C. *J. Catal.* **1998**, *175*, 294.
(4) Yokoyama, C.; Misono, M. *J. Catal.* **1994**, *150*, 9.
(5) Bethke, K. A.; Li, C.; Kung, M. C.; Yang, B.; Kung, H. H. *Catal. Lett.* **1995**, *31*, 287.
(6) Sumiya, S.; He, H.; Abe, A.; Takezawa, N.; Yoshida, K. *J. Chem. Soc. Faraday Trans.* **1998**, *94*, 2217.
(7) Kameoka, S.; Ukisu, Y.; Miyadera, T. *Phys. Chem. Chem. Phys.* **2000**, *2*, 367.
(8) Shimizu, K.; Shibata, J.; Yoshida, H.; Satsuma, A.; Hattori, T. *Appl. Catal. B* **2001**, *30*, 151.
(9) Shimizu, K.; Satsuma, A.; Hattori, T. *Appl. Catal., B* **2000**, *25*, 239.
(10) Burch, R.; Breen, J. P.; Meunier, F. C. *Appl. Catal., B* **2002**, *39*, 283.
(11) Meunier, F. C.; Breen, J. P.; Zuzaniuk, V.; Olsson, M.; Ross, J. R. H. *J. Catal.* **1999**, *187*, 493.
(12) Sumiya, S.; Saito, M.; He, H.; Feng, Q.-C.; Takezawa, N. *Catal. Lett.* **1998**, *50*, 87.
(13) Kameoka, S.; Chafik, T.; Ukisu, Y.; Miyadera, T. *Catal. Lett.* **1998**, *55*, 211.
(14) Shimizu, K.; Kawabata, H.; Satuma, A.; Hattori, T. *Appl. Catal., B* **1998**, *19*, L87.
(15) Shimizu, K.; Kawabata, H.; Satsuma, A.; Hattori, T. *J. Phys. Chem. B* **1999**, *103*, 5240.
(16) Mack, H. G.; Della Vedova, C. O.; Wellner, H. *J. Mol. Struct.* **1993**, *291*, 197.
(17) Koga, Y.; Nakanaga, T.; Sugawara, K.; Watanabe, A.; Sugie, M.; Takeo, H.; Kondo, S.; Matsumura, C. *J. Mol. Spectrosc.* **1991**, *145*, 315.
(18) Joo, D.-L.; Merer, A. J.; Clouthier, D. J. *J. Mol. Spectrosc.* **1999**, *197*, 68.
(19) Hawkins, M.; Andrews, L. *J. Am. Chem. Soc.* **1983**, *105*, 2523.
(20) Rodler, M.; Blom, C. E.; Bauder, A. *J. Am. Chem. Soc.* **1984**, *106*, 4029.
(21) Saito, S. *Chem. Phys. Lett.* **1976**, *42*, 399.
(22) Rodler, M.; Bauder, A. *J. Am. Chem. Soc.* **1984**, *106*, 4025.